Experimental Techniques (2020) 44:597–612
https://doi.org/10.1007/s40799-020-00382-9

RESEARCH PAPER

Analysis of Yield Criteria and Flow Curves on FLC for TWIP900 Steel

S. Kilic[1] · F. Ozturk[2,3] · S. Toros[4]

Received: 15 October 2018 / Accepted: 13 May 2020 / Published online: 29 May 2020

Abstract
In this study, the applicability of yield criteria and flow curve models to predict forming limit curve (FLC) via the Marciniak-Kuczynski (M-K) model is investigated for TWIP900 steel. Forming limit characteristics of TWIP900 are determined experimentally and numerically. The yield criteria of Hill48, Barlat89, YLD2000-2d, and BBC2000 are tested and compared with each other. Results indicate that the YLD2000-2d and the BBC2000 yield criteria are found to be more accurate than the other criteria. The YLD2000 criterion has the best prediction capability with the Krupskowsky flow curve while the BBC2000 model has the best prediction with the Ludwick flow curve model.

Keywords Yield criteria · Forming limit curve · TWIP steel · M-K model

Introduction

Fossil fuel reserves in the world have been swiftly decreased and environmental pollution has dramatically increased. Tremendous amount of efforts have been made in many industries to reduce fuel consumption and reduce carbon dioxide emission. The automotive industry is one of the major players on the impact of environmental pollution. Recently, the automotive industry has primarily focused on fuel consumption reduction of the vehicles by lightening the structures, using hybrid systems in which both fossil fuels and electric power are used with together or electric vehicles which also decrease environmental pollution. However, the travel range of these new hybrid systems is a serious limitation and the investments and investigations on the battery technologies have been increased. The lightening of the system components in the automotive industry without sacrificing strength is one of the most important research topics for Original Equipment Manufacturers (OEMs) and scientists from past to present. The light vehicle can easily satisfy environmental regulation, restriction, and minimum emission requirements. Advanced High Strength Steels (AHSS) are a commonly used material group for the structural lightening projects since their thinner forms are able to satisfy the desired safety and formability requirements [1]. It is expected that new generation material groups like AHSS or some special non-ferrous materials in the structural lightening projects will have positive impact on carbon emissions without sacrificing safety or even increasing safety requirements. In the automotive industry, aluminium-magnesium (Al-Mg) alloys and AHSS are widely considered to reduce the weight of the vehicle. In the AHSS group; **D**ual **P**hase (DP), **TR**ansformation **I**nduced **P**lasticity (TRIP), and **TW**inning **I**nduced **P**lasticity (TWIP) steels are the most commonly used materials steels. For example, in a hood construction, the use of DP590 steel with a thickness of 0.55 mm instead of BH340 steel with a thickness of 0.7 mm resulted in a 21% reduction in hood weight [2]. Among these materials, TWIP steels are of interest because of their high mechanical properties and formability. TWIP steels which are the second generation of the AHSS, were developed to provide the weight reduction of the vehicles. In Fig. 1, the general comparison of the steels is displayed with respect to tensile strength vs. elongation. As can be seen in the figure, it is clear that the main target of steel producers is to increase the strength and formability of the materials. Typical applications of TWIP steels in automotive components are, in A-Pillar, wheelhouse, front side member, wheel, lower control arm, front and rear bumper beams, B-

✉ S. Kilic
suleymankilic@ahievran.edu.tr

[1] Department of Mechanical Engineering, Kırşehir Ahi Evran University, Kırşehir, Turkey

[2] Turkish Aerospace Industries, Inc., Ankara, Turkey

[3] Department of Mechanical Engineering, Ankara Yıldırım Beyazıt University, Ankara, Turkey

[4] Department of Mechanical Engineering, Omer Halisdemir University, Niğde, Turkey

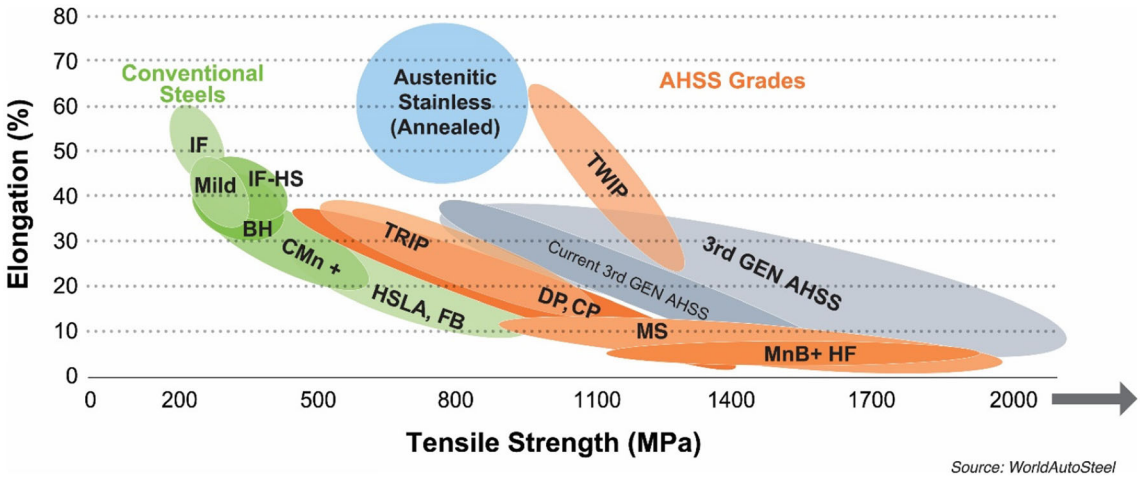

Fig. 1 Comparison of the mechanical properties of the steels for automotive industry [1]

pillar, wheel rim, floor cross-member, wheelhouse, door impact beam [3].

Since AHSS are relatively new materials, more detailed experimental and numerical works are required to determine the formability characteristics. In this group, TWIP is a steel with an austenite phase containing high manganese content which causes a high stacking fault energy [4]. The primary deformation mechanism in TWIP steels involves shear dislocation and twinning which occurs at high strength (>800 MPa) [5, 6]. In addition, due to the high hardening capability, necking is delayed through plastic deformation. As a result, because of high elongation values (>40%), highly complex shaped parts can be produced without any failure [7]. However, TWIP steels have also some disadvantages through the forming operations like high amount of springback [8] and forming forces. Early version of the TWIP steels had also delayed crack phenomena which were a serious problem for the OEMs products and this problem was solved by the addition of aluminium [9].

The modelling of forming characteristics of the TWIP steels is another main research interest since their behaviour under different deformation mode is more complex than the other conventional steels. As previously mentioned, during the forming process of these steels that may reach 800 MPa strength and higher, twinning mechanism, which affects the hardening characteristics of the materials, occurs in the microstructure. Therefore, the classical hardening models are insufficient to represent the material's behaviour within the given plastic deformations. Information about the forming limits of TWIP steels is very scarce at different conditions in the literature. Chung et al. [10] experimentally obtained the forming limit diagram of the TWIP940 steel and studied the various models' estimation performance. They showed that the predicted FLD by the Marciniak-Kuczynsky (M-K) instability model shows higher prediction than the experimental FLD curve. However, in the same study, the model for DP600 material showed a lower estimation. This indicates that the selected models and their parameters, which reflect the materials' behaviours, must be carefully investigated for TWIP steels. Traditional selection method may not work for TWIP steel. Since the instability models include the hardening model and/or yield criteria, more complex models have to be developed to better predict material behavior. Habibi et al. [11] investigated the experimental FLD of TWIP steel (Fe-19-795Mn-2Al-0.6C) and modelling issues of the forming limits with several fracture criteria. The simple ductile or shear fracture criteria are not satisfactory for modelling of the forming limits of the TWIP steel. However, models like those developed by Han-Kim [12] and Lou [13] which contain both shear and normal stress effects, predict the formability more accurately. Xu et al. [14] determined the yield surface of the TWIP980 steel experimentally and numerically. They showed that the YLD2000 model has a good agreement with the experiment. In an another study, the yield surface of the TWIP1000 steel was also determined experimentally and the success of the YLD2000 model was once again shown in comparison for model estimations [15]. Selected yield criteria for the instability models to determine the forming limit of the materials are quite important to evaluate the hardening and springback characteristics of the materials. Ahn et al. [16] studied the springback characteristics of the TWIP steel experimentally and numerically. In the numerical works, kinematic and isotropic hardening models with the YLD2000 yield function were used to evaluate the springback characterization of the TWIP steel. They showed that the hardening models have a small effect on springback simulation results.

In this study, the performance of the frequently used yield criteria in finite element simulations of the stamping operations was evaluated for TWIP900 steel. The model coefficients of the Hill48 [17], the Barlat89 [18], the YLD2000 [19] and the BBC2000 [20] yield criteria were determined by tensile test samples prepared at different orientations (0°,

15°, 30°, 45°, 60°, 75°, 90°). Additionally, forming limit characteristics of TWIP900 were also determined experimentally and numerically. Through the numerical studies of the forming limit curves, the M-K instability criteria were used with the yield criteria. The most appropriate yield criteria for the TWIP900 was identified.

Materials and Methods

Materials

In this study, commercially available TWIP900 CR steel sheet with a thickness of 1.3 mm was studied. CR initials indicate cold rolling operation. Tensile test samples were prepared by laser cutting machine according to ASTM E8 standard. It is well-known that TWIP steels consist of fully austenite phases and microstructural view obtained from the optic microscope (Olympus BX-51) is illustrated in Fig. 2. The samples were etched in a 5% Nital solution to visualize the austenite phases. Average grain size was determined as 5.65 μm by the image analyzer which is implemented into microscope software. Chemical composition of the material is determined and summarized in Table 1.

Tensile tests

Tensile samples were prepared at different orientations that are 15° angle with respect to rolling direction (RD). The samples were tested at a deformation speed of 25 mm/min using Shimadzu Autograph AGIS-100 kN tensile testing machine. Each test was repeated at least three times and average values were determined. Deformations were measured by a video extensometer. This system consists of two cameras and a software which detects the amount of displacement of the lines drawn on the surfaces of the samples with an accuracy of 0.1%. The system works on the measurement of the motion of the lines within the frame of two separate cameras during the test (as long as the sample is extended). The gauge lengths of the samples were set to 50 mm at the initial stage of the experiments.

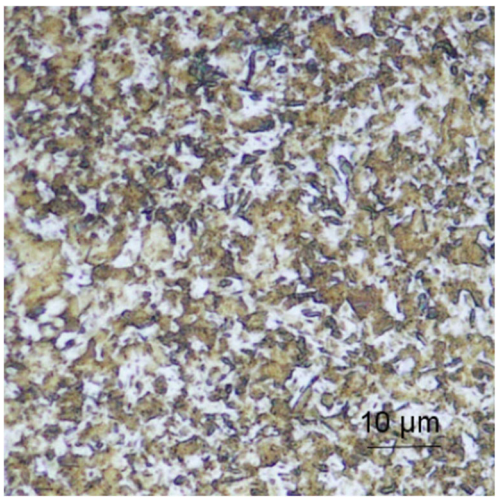

Fig. 2 The optical image of the TWIP900 steel

Table 1 Chemical composition of TWIP900 CR sheet (in wt.%)

C	Mn	Si	Cr	Al	Fe
0.37	20.96	0.17	0.46	4.80	Balance

Determination of anisotropy

In sheet metal forming processes, the anisotropic behaviour, one of the important material properties in the view of the formability, should be determined. Anisotropy is the change of material properties depending on the selected direction and indicated by R or r. Sheet metals have two different anisotropic behaviours namely planar and normal anisotropies, which give information about the formability characteristics of materials. Planar anisotropy means that sheet metal has different mechanical properties along its plane while the normal anisotropy is the variation of the properties through the thickness. In addition, high planar anisotropy values usually cause wrinkling and ear formation on the sheet metals. An anisotropy parameter namely Lankford's parameter is calculated by the ratio of the strains at width to thickness of the sheet metal, as given in Eq. (2.1). ($\varepsilon_w$and $\varepsilon_t$are the strain in the width and thickness direction)

$$r = \frac{\varepsilon_w}{\varepsilon_t} \tag{2.1}$$

In most cases, since the measurement of deformation through the thickness is not an easy task, it is calculated according to the volume constancy principle as given in Eq. (2.2). Finally, the Lankford's parameters are obtained by Eq. (2.3). ($\varepsilon_l$is the strain in the length direction)

$$d\varepsilon_l + d\varepsilon_w + d\varepsilon_t = 0 \tag{2.2}$$

$$r = \frac{\varepsilon_w}{\varepsilon_t} = \frac{\varepsilon_w}{-\varepsilon_w - \varepsilon_l} \tag{2.3}$$

The difference between the anisotropy values at different orientations is mainly attributed to orientation of the grains with respect to the rolling direction of the sheet metals. Therefore, in order to determine the anisotropic properties of the TWIP900 steel, tensile test specimens were prepared in different directions (0°, 15°, 30°, 45°, 60°, 75°, 90°) from a sheet sample as shown in Fig. 3. The purpose of these experiments is to determine performance of the anisotropic yield criteria using the Hill48, Barlat89, YLD2000, and BBC2000

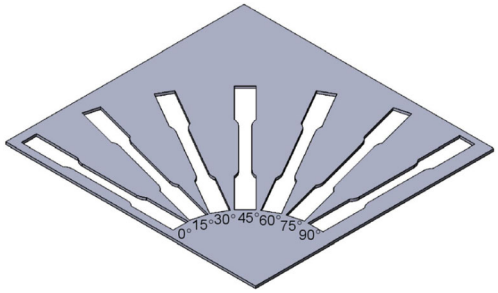

Fig. 3 Illustration of test samples prepared with a 15° angle with respect to RD.

that include the anisotropic parameters. Some investigators [10] have studied 0°, 45° and 90° directions of TWIP940, TWIP980, and TWIP1000 steels. More studies are needed in other directions to get the most accurate results. Therefore, more detailed experimental investigations were carried out in this study.

In the process of the measuring anisotropy, image-processing technique was used. In the used program, measurement was made by using a reference cube whose dimensions were known. Before the test, the first measurements were made manually by means of calipers and micrometers. Afterwards, the first photo was taken, its accuracy was checked and then experiments were started. At least 8 photographs were taken during each experiment. Thus, the total number of photos in one direction was at least 24. Two different correlation methods are performed to determine the measurement precision of the used DIC system. In the first method, the measured deformations via DIC system were compared with the video extensometer that belongs to tensile test system for the specified stroke levels in the longitudinal direction. The measurement methods and deformations are depicted in Fig. 4 (a,b) respectively for both DIC systems. As can be seen from the Fig. 4b, the deformations are very close to each other. After the confirmation work of the DIC system, the deformations through the transverse directions were measured via the same DIC system. In addition, the deformations at the transverse directions were also measured via the micrometer (Fig. 4d) for the last stage of the deformations. The results show good agreement with the micrometer measurements.

Biaxial anisotropy

The anisotropy values are generally determined by a simple tensile test. However, in real forming processes, the deformations mostly occur biaxially rather than uniaxially. Therefore, it is necessary to determine the anisotropic properties of a sheet material under biaxial loading condition. In literature, biaxial drawing [21] or disc compression [22] tests are performed to determine the biaxial anisotropy value r_b. In this study, biaxial anisotropy was assessed using a hole expansion test [23, 24]. In this process, a hole with a diameter of 25 mm is machined to the center of sheets that have 200 × 200 mm dimensions. The hole expansion tests were performed via the MTS forming device which has a diameter of 50 mm punch. A series of photos were taken until the occurrence of the crack on the samples and finally, the photos were transferred to the image analyzer software to measure the deformations. The unit deformations in the 1 and 2 directions were measured by image processing techniques using the photographs immediately before cracking of the specimen. A hollow punch was used to reduce the frictions between the punch and blank as shown in Fig. 5a. The expanded hole's diameters were measured through the rolling and transverse directions by image analyzing methods. In Fig. 5b, the formed sample and measurement lines were depicted. In this method, it is also possible to determine the Lankford's parameters of the materials under tensile loading conditions for all prescribed directions.

Experimental FLC

In this study, a semi-spherical (out-of-plane) test was used to determine the forming limit curve (FLC) of TWIP900 CR steel. A schematic view of the experiment is given in Fig. 6.

The samples with different geometries are prepared in order to determine the forming limits at different deformation modes. The dimensions of the FLC samples are given in Fig. 7 [25]. The width of the test specimens varies from 25 mm to 200 mm with increments of 25 mm. Geometric differences in the samples lead to have different deformation modes ranging from uniaxial tensile to biaxial stretching. The FLC of material is generally constructed by drawing a curve passing through these different necking points.

An image processing technique was used similarly to the anisotropy measurements in order to determine the strains on the deformed samples. Prior to the deformation of the samples, 2.5 × 2.5 mm^2 grids were etched on the surfaces of the samples by the serigraphy method. Then the samples were deformed with a semi-spherical punch at a deformation rate of 25 mm/min. ASAME (Automated Strain Analysis and Measurement Environment) [26] software technology in which a reference measurement cube was used to measure the deformations of square grids on deformed regions, helps on constructing the forming limit curves of the sheet materials. In Fig. 8 (a and b), the deformation measurement technique [27] and the deformed samples of TWIP900 steel are illustrated, respectively.

Yield criteria

The yield surface is a diagram shows the initiation of the plastic deformation of the materials under various deformation modes that occurs through the forming operations. Although a yield point (critical stress value for the initial plastic

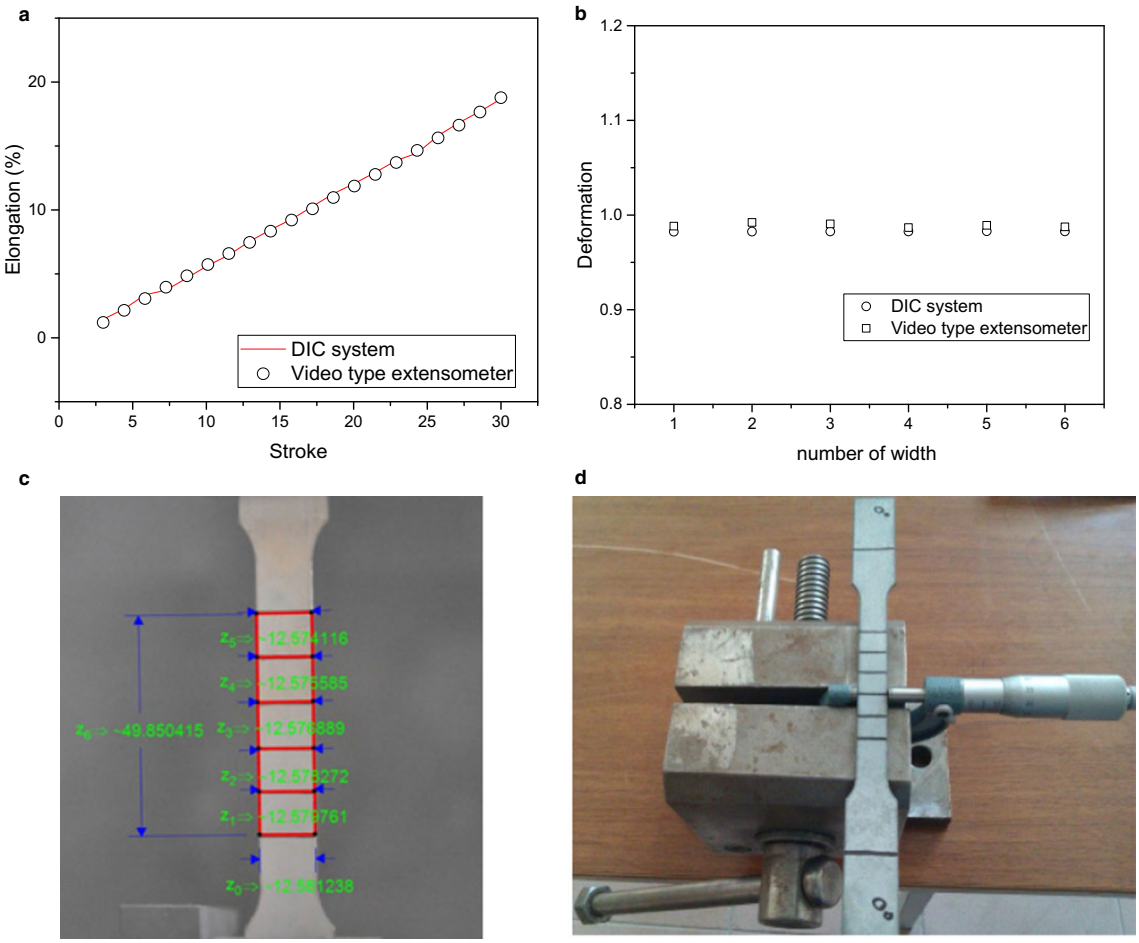

Fig. 4 **a)** The measurement methods, **b)** Deformations **c)** Measuring the width and the height of the test sample via image-processing method, **d)** measuring via the micrometer

deformation) can be determined via a simple tensile test for a one-dimensional loading condition, it is not easy to determine for multi-axial loading conditions particularly for anisotropic sheet metals. For this purpose, either multi-axial loading test devices must be used or advanced anisotropic yield criteria must be evaluated to determine the initiation of the plastic deformation which belongs to the selected loading conditions. A simple yield surface with loading conditions is shown in Fig. 9. Here, the area inside the ellipse indicates that the plastic deformation has not yet started, and the outside area indicates that the plastic deformation has occurred.

Determination of the yield surface is important for the detection of the point at which the plastic deformation begins. These surfaces can be predicted by yield criteria that involve

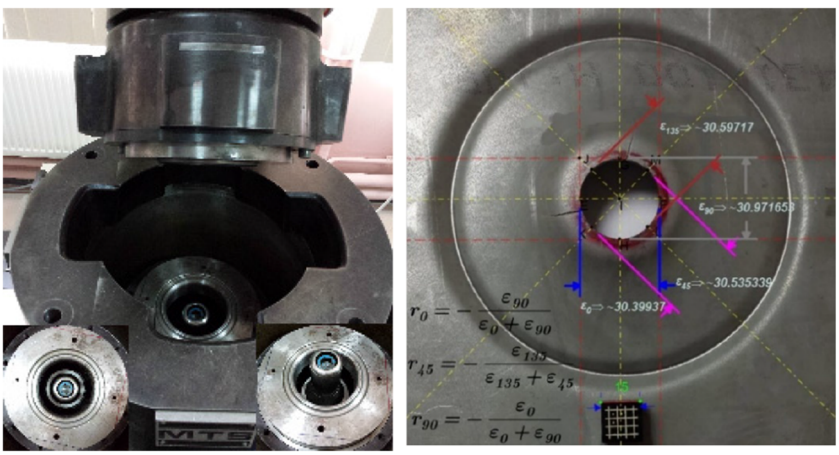

Fig. 5 (a) MTS model forming machine, (b) Formed sample

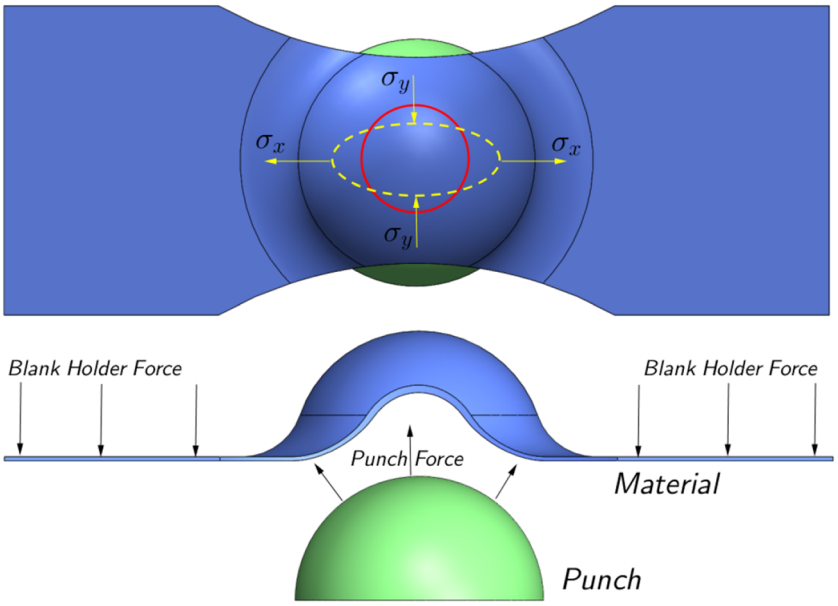

Fig. 6 Schematic representation of the forming limit curve test

the Lankford's parameters and yield stress values determined from tensile tests of samples taken from different directions of the material. The yield criteria are also used in the calculation of the plastic strain increments through the forming simulations.

Sheet materials generally exhibit anisotropic behavior because they are rolled products and mechanical properties change with the orientation of grains. Tresca [28] and von Mises [29], the first and well-known yield criteria, have identified yield surfaces with the assumption that the materials are isotropic. In the following years, it has been understood that the anisotropic behavior of the materials cannot be represented by such isotropic yield criteria. Therefore, new yield criteria that include the anisotropic features of the materials have been proposed. In this study, Hill48 [17], Barlat89 [18], YLD2000 [19], and BBC2000 [30] anisotropic yield criteria were used to evaluate the yield surface of TWIP900 CR steel.

Hill48 yield criterion

This anisotropic yield criterion is commonly used in finite element programs that implement the general form of Eq. (2.4),

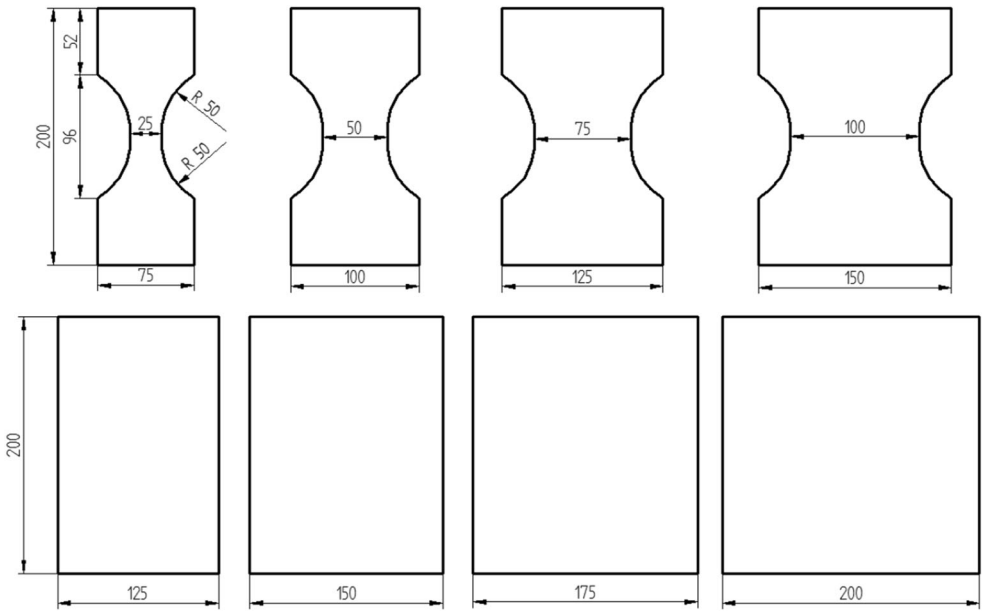

Fig. 7 FLC samples geometries [25]

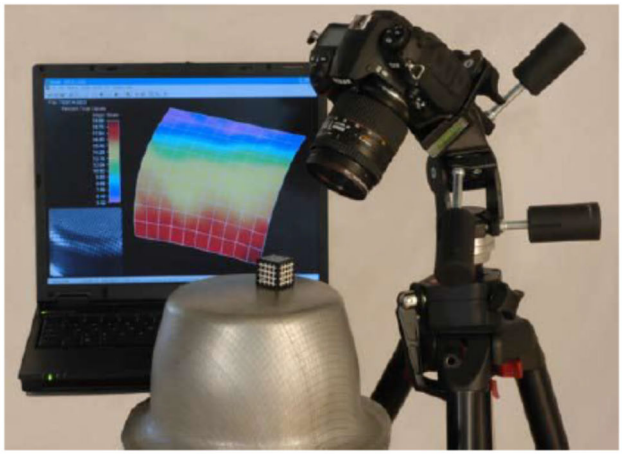

a

b

Fig. 8 (a) Grid measurement system [25], (b) Deformed FLC samples of TWIP900 steel

$$2f(\sigma_{ij}) = F(\sigma_{22}-\sigma_{33})^2 + G(\sigma_{33}-\sigma_{11})^2 + H(\sigma_{11}-\sigma_{22})^2 + 2L\sigma_{23}^2 + 2M\sigma_{31}^2 + 2N\sigma_{12}^2 = 1 \tag{2.4}$$

In the equation σ_{11}, σ_{22}, σ_{33}, σ_{12}, σ_{23}, σ_{31} are the stress tensor components and *F, G, H, L, M,* and *N* are the anisotropic model coefficients. The above expression can be also written under the plane stress condition as in Eq. (2.5).

$$2f(\sigma_{ij}) = (G+H)\sigma_{11}^2 - 2H\sigma_{11}\sigma_{22} + (F+H)\sigma_{22}^2 + 2N\sigma_{12}^2 = 1 \tag{2.5}$$

In Equation (2.6), *G*, *H*, *F,* and *N* coefficients can be calculated by using the experimentally determined anisotropy values (r_0, r_{45}, r_{90}).

$$\begin{aligned} F &= \frac{r_0}{r_{90}(1+r_0)} \\ G &= \frac{1}{(1+r_0)} \\ H &= \frac{r_0}{(1+r_0)} \\ N &= \frac{(r_0+r_{90})+(1+2r_{45})}{2r_{90}(1+r_0)} \end{aligned} \tag{2.6}$$

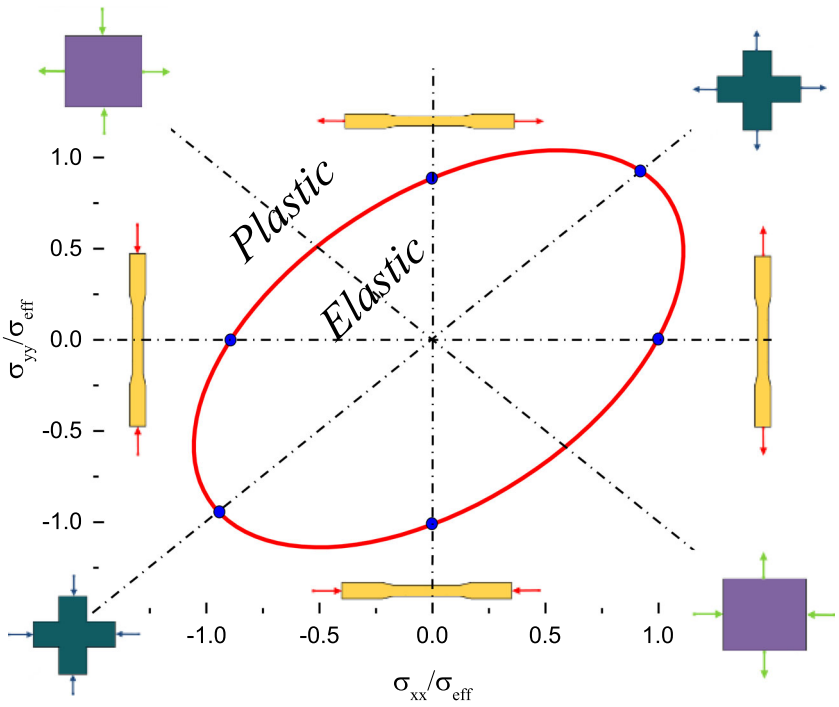

Fig. 9 Schematic representation of a typical yield surface

Barlat89 yield criterion

The model presented by Barlat is given in Equation (2.7).

$$f = a|k_1 + k_2|^M + a|k_1 - k_2|^M + c|2K_2|^M = 2\overline{\sigma}^M \tag{2.7}$$

Where k_1 and k_2 are tensile tensor invariants and are calculated as follows.

$$\begin{aligned} k_2 &= \sqrt{\left(\frac{\sigma_x + h\sigma_y}{2}\right)^2 + p^2\tau_{xy}^2} \\ k_2 &= \sqrt{\left(\frac{\sigma_x + h\sigma_y}{2}\right)^2 + p^2\tau_{xy}^2} \end{aligned} \tag{2.8}$$

The parameters *a, c,* and *h* are also determined by means of Equations (2.9) using the anisotropy values (r_0, r_{90}) determined experimentally. (Details for these parameters can be found in Ref. [18])

$$\begin{aligned} a = 2 - c &= 2 - 2\sqrt{\frac{r_0}{1+r_0}\frac{r_{90}}{1+r_{90}}} \\ h &= \sqrt{\frac{r_0}{1+r_0}\frac{1+r_{90}}{r_{90}}} \end{aligned} \tag{2.9}$$

YLD2000 yield criterion

This criterion developed by Barlat requires minimum 8 parameters which are determined experimentally. These parameters are Lankford's parameters (r_0, r_{45}, r_{90}, r_b) and yield strength values (σ_0, σ_{45}, σ_{90}, σ_b) at different directions. The general form is given in Equation (2.10).

$$\phi = \phi' + \phi'' = 2\sigma^a \tag{2.10}$$

ϕ' and ϕ'' are the stress state that calculated by the principle deviatoric stresses as given in Equation (2.11).

$$\begin{aligned} \phi' &= |S_1 - S_2|^a \\ \phi'' &= |2S_2 + S_1|^a + |2S_1 + S_2|^a \end{aligned} \tag{2.11}$$

The Equation (2.10) can be also evaluated by the linear transformation of the normal stresses that are expressed in Equation (2.12) or (2.13).

$$\phi = \phi'\left(X'\right) + \phi''\left(X''\right) = 2\sigma^a \tag{2.12}$$

$$\phi' = \left|X_1' - X_2'\right|^a \tag{2.13}$$

$$\begin{aligned} \phi'' &= \left|2X_2'' - X_1''\right|^a + \left|2X_1'' - X_2''\right|^a \\ X' &= C's = C'T\sigma = L'\sigma \\ X'' &= C''s = C''T\sigma = L''\sigma \end{aligned} \tag{2.14}$$

In Equation (2.10), a is taken as 6 according to the Hosford's suggestion for FCC materials. In the Equation (2.14) L' and L'' are the coefficients that involve 8 anisotropy parameters $\alpha_1 - \alpha_8$ are given in Equation 2.15 and 2.16.

$$\begin{bmatrix} L_{11}' \\ L_{12}' \\ L_{21}' \\ L_{22}' \\ L_{66}' \end{bmatrix} = \begin{bmatrix} 2/3 & 0 & 0 \\ -1/3 & 0 & 0 \\ 0 & -1/3 & 0 \\ 0 & 2/3 & 0 \\ 0 & 0 & 1 \end{bmatrix} \begin{bmatrix} \alpha_1 \\ \alpha_2 \\ \alpha_7 \end{bmatrix} \tag{2.15}$$

$$\begin{bmatrix} L_{11}'' \\ L_{12}'' \\ L_{21}'' \\ L_{22}'' \\ L_{66}'' \end{bmatrix} = \frac{1}{9}\begin{bmatrix} -2 & 2 & 8 & -2 & 0 \\ 1 & -4 & -4 & 4 & 0 \\ 4 & -4 & -4 & 1 & 0 \\ -2 & 8 & 2 & -2 & 0 \\ 0 & 0 & 0 & 0 & 9 \end{bmatrix} \begin{bmatrix} \alpha_3 \\ \alpha_4 \\ \alpha_5 \\ \alpha_6 \\ \alpha_8 \end{bmatrix} \tag{2.16}$$

BBC2000 yield criterion

The BBC2000 yield criterion is another anisotropic yield criterion, which is developed with adding two different coefficients to the Barlat89 yield criterion. The anisotropic parameters are calculated with 8 experimental values r_0, r_{45}, r_{90}, r_b, σ_0, σ_{45}, σ_{90}, σ_b and general form of the criterion is given in Equation 2.17.

$$\overline{\sigma} = \left[a|b\Gamma + c\psi|^{2k} + a|b\Gamma - c\psi|^{2k} + (1-a)|2c\psi|^{2k}\right]^{\frac{1}{2k}} \tag{2.17}$$

In this equation *a, b, c,* and *k* are material parameters where k is 3 in BCC alloys and 4 in FCC alloys. Therefore, it was taken as 4 in the calculations for TWIP steel.

In addition, Γ and ψ are the stress state expressed in terms of the second and third invariants of a transformed stress tensor.

$$s_{11}' = d\sigma_{11} + e\sigma_{22} \tag{2.18}$$

$$s_{22}' = e\sigma_{11} + f\sigma_{22} \tag{2.19}$$

$$s_{33}' = -(d+e)\sigma_{11} - (e+f)\sigma_{22} \tag{2.20}$$

$$s_{13}' = s_{23}' = 0 \tag{2.21}$$

The coefficients *d, e, f,* and *g* in Equation (2.18–2.21) are the anisotropy coefficients of the material. Γ and ψ can be calculated in terms of the stress components, σ_{11}, σ_{22} and σ_{12} as given in Equation 2.22–23 to reduce the calculation steps.

$$\Gamma = M\sigma_{11} + N\sigma_{22} \tag{2.22}$$

$$\psi = \sqrt{(P\sigma_{11} + Q\sigma_{22})^2 + R\sigma_{12}^2} \tag{2.23}$$

In these equations, *M, N, P, Q,* and *R* are the material parameters that are calculated by the anisotropic coefficients *d*, *e*, *f,* and *g* as given in Equation (2.24).

$$\begin{aligned} \mathrm{M} &= \mathrm{d} + \mathrm{e} \\ \mathrm{N} &= f + \mathrm{e} \\ \mathrm{P} &= \frac{\mathrm{d}-\mathrm{e}}{2} \\ \mathrm{Q} &= \frac{\mathrm{e}-f}{2} \\ \mathrm{R} &= g^2 \end{aligned} \tag{2.24}$$

A minimization procedure according to experimentally found Lankford parameters and yield stresses with respect to the selected orientations and biaxial conditions was applied for calculating the anisotropic coefficients of both the YLD2000 ($\alpha_1 - \alpha_8$) and BBC2000 (*a, b, c, d, e, f,* and *g*) yield criteria. In this study, the biaxial stress was determined by the Equation (2.25) (Details for this equation can be found in Ref.) [31].

$$\sigma_{biaxial\ flow} = \sigma_{uniaxial\ flow}\sqrt{\frac{(1+r_0)r_{90}}{r_0 + r_{90}}} \tag{2.25}$$

The performance of the yield criteria on representing the material properties can be evaluated by the calculation of the anisotropy and yield strength values with respect to the experimentally tested directions. In general form, the stresses that occurred for the selected orientations can be calculated by the Equation (2.26). In the given equation, F_θ is a function of anisotropy coefficients and the related trigonometric expressions while Y_θ refers to yield stress of the sample at different angles with respect to the rolling directions.

$$\sigma = Y_\theta F_\theta \tag{2.26}$$

$$\begin{aligned} \sigma_{11} &= Y_\theta cos^2\theta \\ \sigma_{22} &= Y_\theta sin^2\theta \\ \sigma_{12} = \sigma_{21} &= Y_\theta sin\theta cos\theta \end{aligned} \tag{2.27}$$

$$Y_\theta = \frac{\overline{\sigma}}{F_\theta} \tag{2.28}$$

Besides the yield stresses at different orientations, the anisotropy values were also calculated according to the Equation (2.29) to check the model performance. In the equation, $\overline{\sigma}$ is the equivalent stress function that was described by the yield criterion.

$$r_\theta = \frac{F_\theta}{\frac{\partial\overline{\sigma}}{\partial\sigma_{11}} + \frac{\partial\overline{\sigma}}{\partial\sigma_{22}}} - 1 \tag{2.29}$$

Modelling of Forming Limit Curve (FLC)

There are many studies in the literature on modelling of the forming limit curves via simple test results such as hardening exponent, strength coefficient, and anisotropic parameters. Among these studies, Marciniak [32] and Marciniak and Kuczynski [33] (M-K model) are the most famous models which are based on geometric irregularity or imperfections of the sheets prior to the deformations. According to M-K model, sheet metal has geometrical imperfections (thickness inhomogeneity) and structural defects (voids etc.) during its production. In the forming processes, these defects expand over time, start to initiate necking, and completely localized on a specific region of the parts during the plastic deformation. Azrin and Backofen [34] experimentally demonstrated the realism of this Marciniak hypothesis. The reason that this model is used extensively and continuously developed by researchers is to have an intuitive background, to accurately estimate the effect of different conditions and material parameters, and to be easily adapted to sheet metal forming simulation programs at the same time. Experimental investigations have shown that necking begins at inhomogeneous structural or geometric disturbances region [32]. The variation in thickness is expressed as inhomogeneity. Although the thickness variation of the sheets occurs very sensitively in reality, in theoretical calculations, it seems like a sudden decrease for a local region. The illustration of the theoretical approach is given in Fig. 10 [35].

As can be seen from Fig. 10, the geometry is examined in two parts: zone "*a*" has a homogeneous thickness t_0^a and inhomogeneous zone "*b*" thickness is t_0^b. Here, the thickness

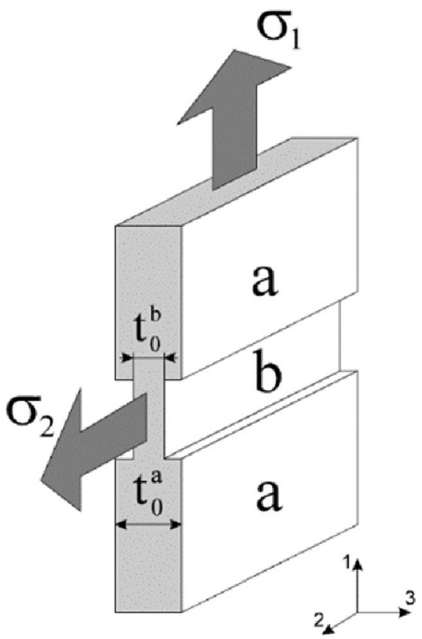

Fig. 10 Geometric representation of the M-K model [35]

ratios are expressed as $f_0 = \left(t_0^a/t_0^b\right)$. At the same time, stresses and unit deformations are examined in two sections $\sigma_1^a, \sigma_1^b, \sigma_2^a, \sigma_2^b$ and $\varepsilon_1^a, \varepsilon_1^b, \varepsilon_2^a, \varepsilon_2^b$. Under these conditions, when the strain ratio, $\varepsilon_1^b/\varepsilon_1^a$ reaches a critical value such as 10, it is assumed that the material starts necking. In the first step of calculation, force balance must be provided to continue the plastic deformation and it is described for the two regions as follows;

$$\begin{aligned} F_{nt}^a &= F_{nt}^b \\ F_{nn}^a &= F_{nn}^b \end{aligned} \tag{2.30}$$

Here F_{nn} and F_{nt} refer to normal and parallel (shear forces that affect the material and the states of stresses in the "*a*" and "*b*" regions of geometry are defined;

$$\begin{aligned} \sigma_{nt}^a \exp\left(\varepsilon_3^a\right) t_0^a &= \sigma_{nt}^b \exp\left(\varepsilon_3^b\right) t_0^b \\ \sigma_{nn}^a \exp\left(\varepsilon_3^a\right) t_0^a &= \sigma_{nn}^b \exp\left(\varepsilon_3^b\right) t_0^b \end{aligned} \tag{2.31}$$

In the early version of the M-K model, the direction of the imperfection is assumed as the perpendicular or parallel to applied loads. Hutchkinson and Nale [34] improved the calculation steps of the M-K model for different orientations of the grooves on the sheet metals. The improved form of the model is illustrated in Fig. 11 [36].

Here, σ_{nn} and σ_{nt} express the stresses in the directions of " n " and " t " . The thickness variation in "*a*" and "*b*" regions of geometry is given by Equation 2.32 in relation to the initial disturbances (f_0).

$$f = f_0 exp\left(\varepsilon_3^b - \varepsilon_3^a\right) \tag{2.32}$$

ε_3 shows the strain value in the direction of thickness which can be calculated according to the principle of volume constancy and is given in Equation 2.33.

$$\varepsilon_3 = -(\varepsilon_1 + \varepsilon_2) \tag{2.33}$$

Equation 2.34 expresses the force equilibrium in terms of the calculated stress values.

$$\begin{aligned} f\sigma_{nt}^b &= \sigma_{nt}^a \\ f\sigma_{nn}^b &= \sigma_{nn}^a \end{aligned} \tag{2.34}$$

The strains developed in the direction "*t*" for both regions were assumed to be equal to the given deformations as described in Equation 2.35.

$$d\varepsilon_{tt}^b = d\varepsilon_{tt}^a \tag{2.35}$$

One of the essential property of the M-K model is to use a yield criterion to describe the plastic strain increments with the given deformations. The relation of the plastic strain increment is expressed in the tensor form in Equation 2.36.

$$d\varepsilon_{ij} = d\overline{\varepsilon}_{ij} \frac{\partial \overline{\sigma}_y}{\partial \overline{\sigma}_{ij}} \tag{2.36}$$

In the model, four unknowns ($\sigma_{nn}^b, \sigma_{tt}^b, \sigma_{nt}^b, d\overline{\varepsilon}$) must be determined using some numerical approach. The Newton-Raphson method is the most commonly used iterative approach to determine the unknowns of the target functions. In the literature, the effective strain increment ($d\overline{\varepsilon}_a$) of the sheet was set to 10^{-4} mm/mm. The relationship between effective stress and strain can be expressed by the following the Ludwik flow curve equation.

$$\sigma(\varepsilon) = \sigma_A + K\overline{\varepsilon}^n \tag{2.37}$$

Here σ_A; yield stress, K; strength coefficient, and n; refers to the strain hardening exponent.

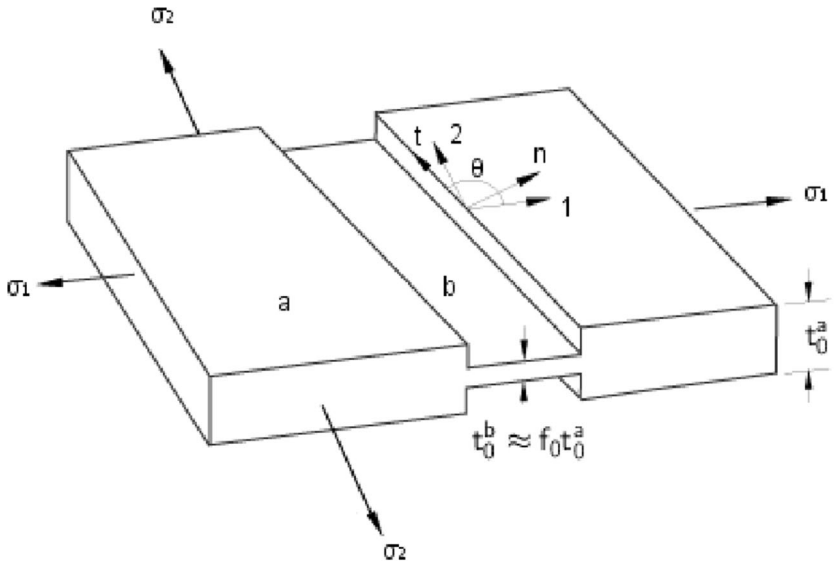

Fig. 11 Improved M-K model [36]

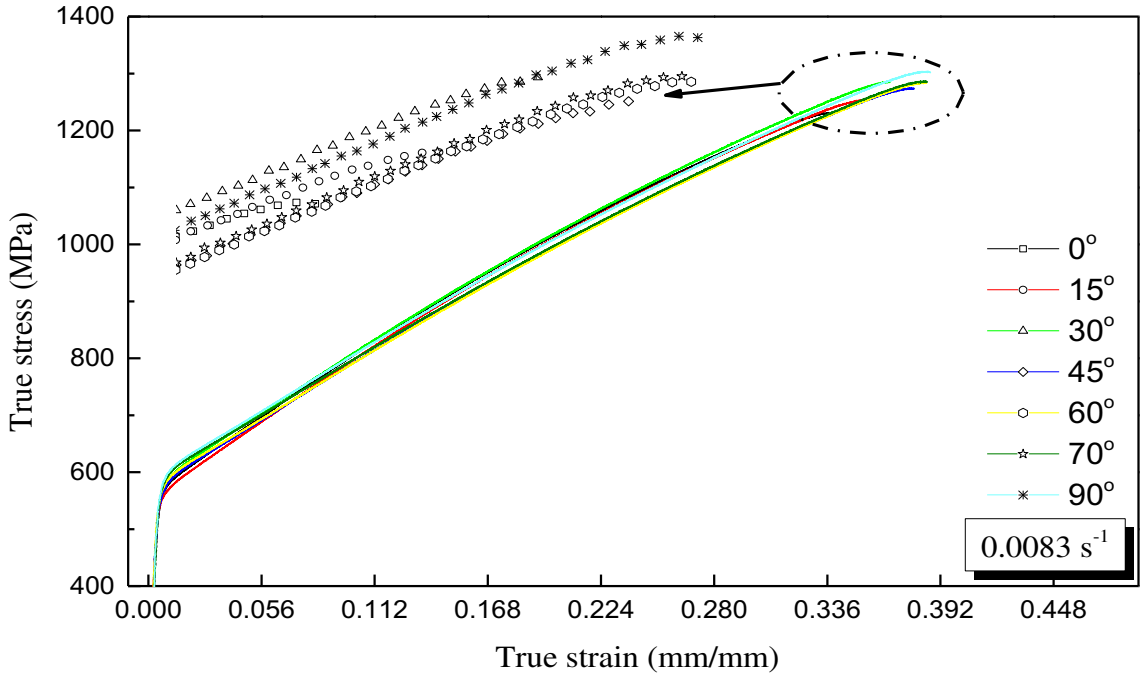

Fig. 12 True stress vs. true strain curves at 0.0083 s^{-1}

In the improved M-K model, the orientation angle of the imperfection should be considered as variable with the given deformation. Therefore, the stresses must be evaluated for each angle to determine the most critical stage of the deformation. A transformation matrix T given in Equation 2.38, is used to express the stresses for the given rotation. Equation 2.39 can calculate the transformed stresses.

$$T = \begin{pmatrix} \cos\theta & \sin\theta \\ -\sin\theta & \cos\theta \end{pmatrix} \tag{2.38}$$

$$\sigma^{ntz} = T\sigma^{xyz}T^{T} = \begin{pmatrix} \sigma_{nn} & \sigma_{nt} \\ \sigma_{nt} & \sigma_{tt} \end{pmatrix} \tag{2.39}$$

Finally, the following equation system (Equation 2.40) must be solved by a numerical procedure in order to calculate the unknown stress and strain values on the representative system. When the critical strain ratio reaches a selected value for a specifically oriented groove, the iteration is cancelled and the final ε_{major} and ε_{minor} are plotted. The detailed description of the numerical procedure is given in [37].

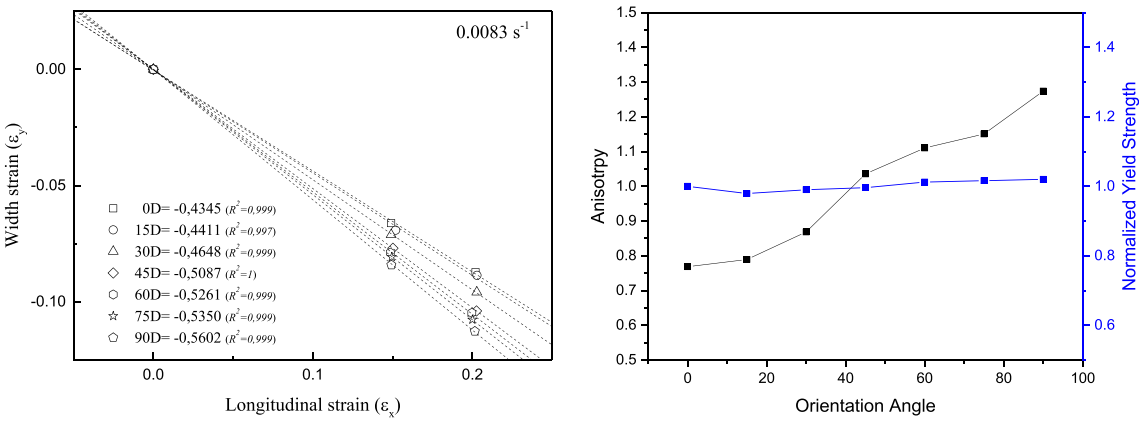

(a) (b)

Fig. 13 **(a)** The slope of the change in width and length, (b)Variation of the Lankford's parameters and normalized yield strength with respect to the orientation angle

Table 2 Mechanical properties of TWIP900 steel

Orientation Angle	*Yield Strength (MPa)*	*UTS (MPa)*	*Uniform Elongation (mm/mm)*	*Total Elongation (mm/mm)*	*n*	*K*	*r*
0°	546	883	0.375	0.406	0.836	1773	0.768
15°	535	884	0.404	0.443	0.829	1769	0.789
30°	541	895	0.421	0.462	0.809	1732	0.868
45°	544	879	0.431	0.477	0.838	1714	1.035
60°	553	883	0.439	0.487	0.843	1708	1.110
75°	555	881	0.429	0.485	0.843	1698	1.151
90°	557	892	0.434	0.485	0.838	1721	1.274

$$F_1 = \frac{d\varepsilon^b_{nn}\sigma^b_{nn} + d\varepsilon^b_{tt}\sigma^b_{tt} + d\varepsilon^b_{nt}\sigma^b_{nt}}{d\bar{\varepsilon}_b\bar{\sigma}_Y} - 1 = 0$$
$$F_1 = \frac{d\varepsilon^b_{tt}}{d\varepsilon^a_{tt}} - 1 = 0$$
$$F_1 = f\frac{\sigma^b_{nn}}{\sigma^a_{nn}} - 1 = 0 \qquad (2.40)$$
$$F_1 = f\frac{\sigma^b_{nt}}{\sigma^a_{nt}} - 1 = 0$$

Results and discussion

The material was tested under different deformation modes. The true stress vs. true strain diagram is shown in Fig. 12 in order to describe material behavior at different orientations. Although the variation of the stress values at plastic deformation region is not too much different, a small fluctuation was obtained for the yield strengths with respect to the different orientations. The yield strength of the material at RD was determined as 546 MPa while the highest one was obtained from the transverse direction and it was determined as 557 MPa. Similarly, the variation of the yield strength with respect to the orientation was plotted with the variation of the Lankford's parameters as shown in Fig. 13.

Another important parameter reflecting the anisotropic behavior of the materials is the Lankford's parameter. In this study, the Lankford parameters were determined by calculating the slope of the variation of the strains in longitudinal and transverse (width) directions as given in Equation (2.3) [10, 16, 38]. The anisotropy tests were carried out at a 0.0083 s^{-1} strain rate. Figure 13 (a) shows the strain variation lines with three specific points (0, 5, 20% strains) for all prescribed orientations. In addition, the slope values of the curves were also given in the figure. It is clearly seen that the slopes of the

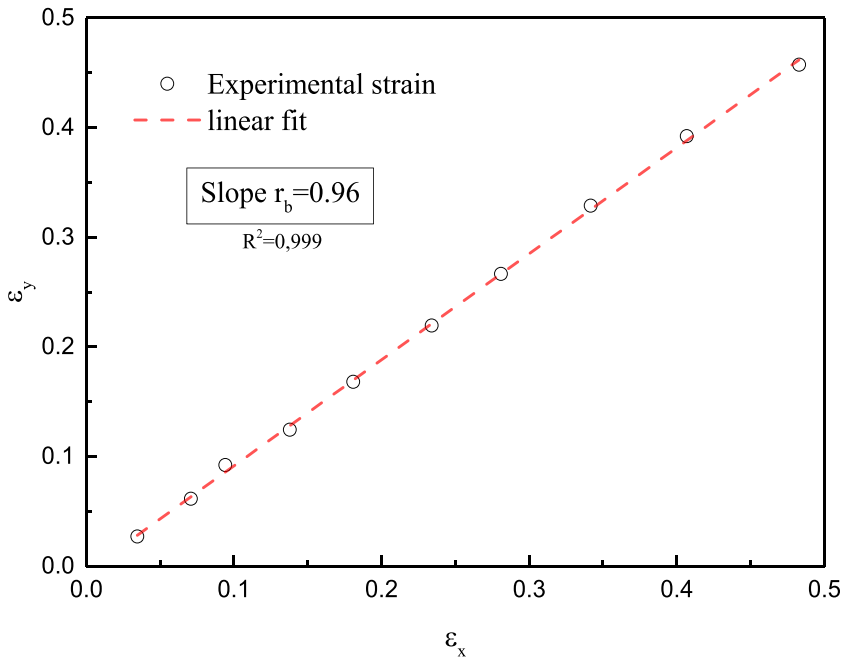

Fig. 14 Biaxial anisotropy of TWIP900 steel

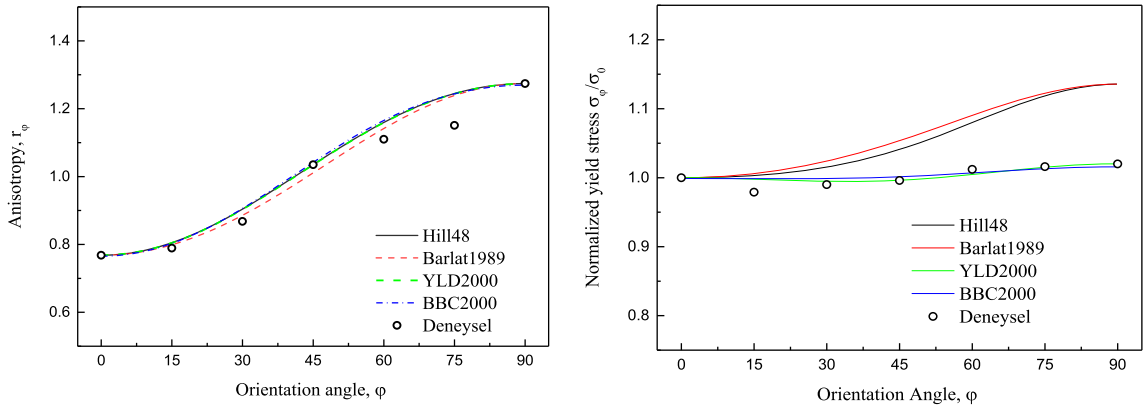

Fig. 15 Prediction capability of the models for anisotropy and yield strength values at different orientations

strains increase with the orientation angle for each sample. This result indicates that the anisotropy increases with orientation angle. The calculated Lankford's parameters were also plotted in Fig. 13b with normalized yield strengths and the values were tabulated with some other important material features in Table 2.

Besides the anisotropy values obtained from the tensile tests, the biaxial anisotropy of TWIP900 steel was determined via hole expansion tests. The biaxial anisotropy value of TWIP900 steel was calculated similarly to the tensile test anisotropy measurement method in which a slope value was used. Here, a slope was found by fitting a linear curve to the obtained unit deformations at rolling and transverse directions. The slope of the fitted curve, namely biaxial anisotropy r_b, was determined as 0.96. The applied method is illustrated in Fig. 14. In addition to the biaxial anisotropy, the biaxial yield strength of TWIP900 steel was calculated according to Equation (2.30) and it was found as 573 MPa. This value was also used to determine the anisotropy parameters of the YLD2000 yield criterion.

There are two methods for determining the suitability of a yield criterion. The first one is to compare the experimental results of a yield surface obtained for different stress combinations. The other one is to compare the experimental anisotropies and yield strengths obtained for the different oriented samples with the model predictions. In this study, experimentally obtained anisotropy and yield strength values were used to evaluate the performance of the studied yield criteria: Hill48, Barlat89, YLD2000, and BBC2000. Although the anisotropic parameters of the Hill48 and Barlat89 can be calculated by the direct use of the Lankford's parameters, a special minimization technique is required for the others, YLD2000 and BBC2000. Actually, although, it is sufficient to determine the anisotropy features of the materials at rolling, diagonal, and transverse directions (r_0, r_{45}, r_{90}) for the studied anisotropic yield criteria, the success of the models on predicting

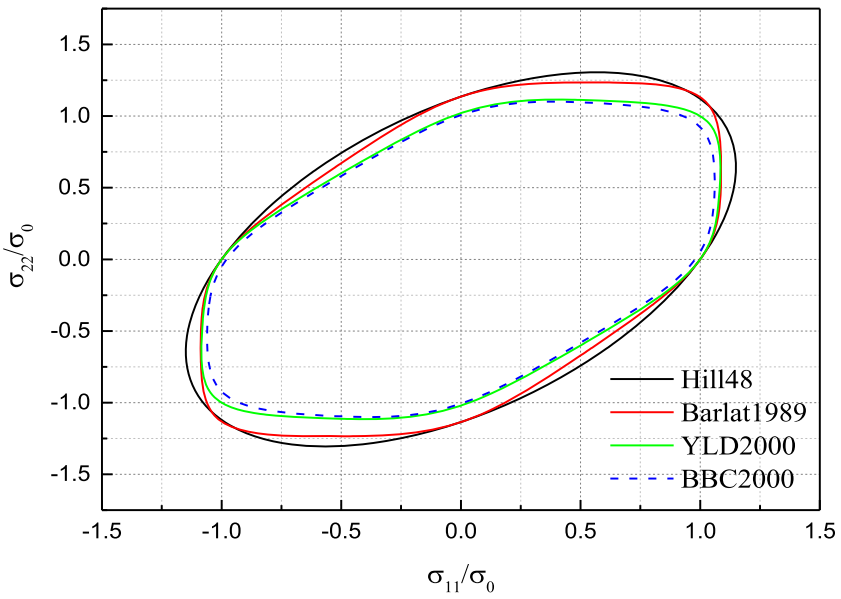

Fig. 16 Estimated yield surfaces for different yield criteria

Table 3 Model coefficients of different yield criteria

Hill48							
F		***G***		***H***		***N***	
0.341		0.5656		0.4344		1.3916	
Barlat1989							
a		***c***		***h***		***p*** (Neglected)	
0.9866		1.0134		0.8805		0.92	
YLD2000-2d							
α_1	α_2	α_3	α_4	α_5	α_6	α_7	α_8
0.9433	1.0333	1.0672	0.9813	1.0059	0.9562	1.0055	1.0037
BBC2000							
a	***b***	***c***	***d***	***e***	***f***		***g***
0.4814	23.6305	3.3831	0.1613	0.1358	−0.0206		0.0211

the other anisotropy and yield strength values were tried to determine. The comparison of the anisotropy and yield stress values predicted by the studied models and experimental data are shown in Fig. 15 (a, b). As can be seen from the figures, although the anisotropy predictions of the models show good agreement with the experimental results, similar achievement could not be obtained for the yield strength prediction at different orientations except for the both YLD2000 and BBC2000 yield criteria. Although the predictions of the Hill48 and the Barlat89 at RD were satisfactory, they have over-estimated the other yield strength values at increasing angle values. The main reason for poor predictions of these two models is that they do not use yield strengths when their anisotropic coefficients are determined.

The predicted yield surfaces of the different models are drawn in Fig. 16 for a constant shear stress value $\sigma_{12} = 0$. As can be seen from the figure, both the Hill48 and the Barlat89 yield criteria predictions are wider than those of the YLD2000 and the BBC2000 yield criteria. This means that the initiation of the plastic deformation begins later for the Hill48 and the Barlat89. Coefficients of yield criteria for TWIP900 steel are listed in Table 3. Since the evaluation of the yield surfaces was made for a constant shear stress, which was assumed as *0*, the parameter *p* in Barlat89 that can be calculated by experimental shear strength or iteratively in numerical approach, was neglected.

In the study, the performances of the anisotropic yield criteria were also evaluated to determine the forming limits of TWIP900 steel with the M-K instability model. In addition, different flow curve models such as the Hollomon, the Ludwick and the Krupskowsky were implemented into the M-K model to calculate the stresses with given strain increment as described earlier. In the study, besides the performances on predicting the forming limits of yield criteria, flow curve models were also evaluated. The flow curve parameters were determined by fitting the models to the experimental true stress vs. true strain data. In this study, instead of plotting the model results, the parameters and statistical errors were tabulated in Table 4. As can be seen from the table, the Ludwick and the Krupskowsky have the best fitting than the Hollomon equation.

In Fig. 17 (a-d), the prediction capabilities of the anisotropic yield criteria and flow cure models for forming limits of TWIP900 steel are depicted. When the predictions are evaluated, it is obviously seen that the used flow curve models have a significant effect on the predicting of the forming limits. As can be seen, the predictions that were obtained by the Hollomon equation are not acceptable for a complexly shaped sheet forming and it predicted the forming limits very low for all anisotropic yield criteria. However, the other flow curve models', the Ludwick and the Krupskowsky, prediction capabilities are more convenient with the experimental forming limit curve as expected.

When the anisotropic yield criteria's performance was evaluated for the prediction of the forming limit curve of TWIP900 steel, the YLD2000 and the BBC2000 have the best prediction capability for both the Ludwick and the Krupskowsky flow curve models. In detail, the YLD2000 has the best prediction with the Krupskowsky flow curve while the BBC2000 has the best prediction with the Ludwick flow curve model.

Conclusion

In this study, mechanical properties of TWIP900 steel were determined and evaluated at different directions. The applicability of the yield criteria and flow curve models to predict the forming limit curve using the M-K model was studied and

Table 4 Flow curve models' parameters

Models	**Equations**	**Parameters**				
		σ_0	**K**	**n**	ε_0	$\mathbf{R^2}$
Hollomon	$\sigma(\varepsilon) = K\varepsilon^n$	–	1636	0.283	–	0.959
Krupskowsky (Swift)	$\sigma(\varepsilon) = K(\varepsilon_0 + \varepsilon)^n$	–	1979	0.622	0.139	0.999
Ludwik	$\sigma(\varepsilon) = \sigma_0 + K\varepsilon^n$	520	1708	0.777		0.999

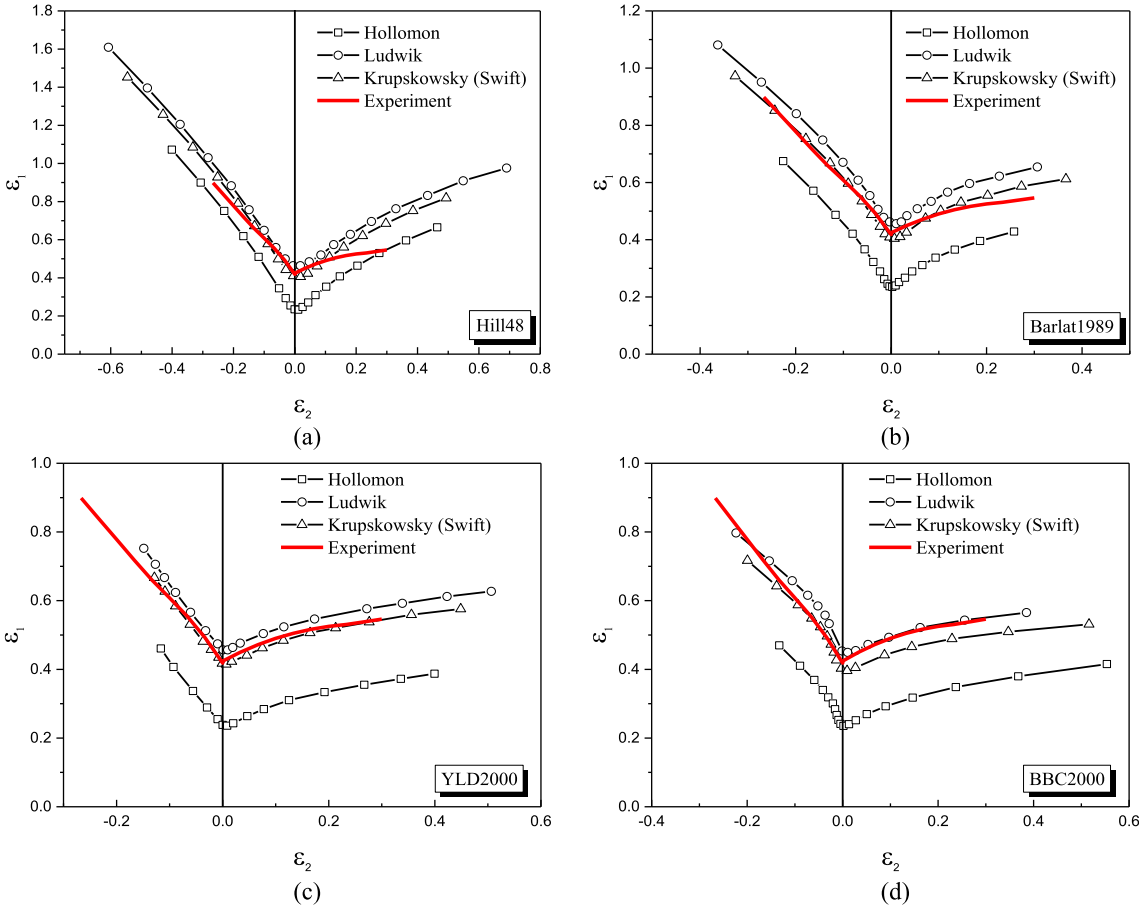

Fig. 17 Effect of different yield criteria flow curve models on predicting the FLC of TWIP900 steel

compared with other anisotropic yield criteria. It was found that the prediction capabilities of the YLD2000 and the BBC2000 models were better than the Hill48, Barlat89 models. Results reveal that the YLD2000 with the Krupskowsky flow model and the BBC2000 with Ludwick flow model were best suited. However, their prediction capabilities on intermediate orientation angles of anisotropy and yield strength were found to be limited.

References

1. Worldautosteel: Steel Your Strength. https://www.worldautosteel.org/why-steel/steel-your-strength/ (Accessed 26 May 2019)
2. Nam, J.B.: Development of new auto steels and application technology. http://309fbf2c62e8221fbaf0-b80c17cbaf20104b072d586b316c6210.r88.cf1.rackcdn.com/Gangzhao%20Presentations/09_China%20Automotive%20Steel%20Conference_POSCO_Jae-Bok%20Nam.pdf (Accessed 2 May 2013). 01.01.2016
3. Singh MK (2016) Application of steel in automotive industry. Int J Emerging Technol Adv Eng 6(7):246–253
4. Schumann VH (1972) Martensitische umwandlung in austenitischen mangan-kohlenstoff-stählen. Neue Hütte 17(10): 605–609
5. Grässel O, Krüger L, Frommeyer G, Meyer L (2000) High strength Fe–Mn–(Al, Si) TRIP/TWIP steels development—properties—application. Int. J. Plasticity 16(10):1391–1409. https://doi.org/10.1016/S0749-6419(00)00015-2
6. Jung J, Lee O, Park Y, Kim D, Jin K, Kim S, Song K (2008) Microstructure and mechanical properties of high Mn TWIP steels. Journal of the Korean Institute of Metals and Materials 46(10):627–633. https://doi.org/10.3390/met7120571
7. Kilic S, Ozturk F, Sigirtmac T, Tekin G (2015) Effects of pre-strain and temperature on bake hardening of TWIP900CR steel. J Iron Steel Res Int 22(4):361–365. https://doi.org/10.1016/S1006-706X(15)30012-1
8. Kiliç S, Öztürk F (2016) Comparison of performances of commercial TWIP900 and DP600 advanced high strength steels in automotive industry. J. Fac. Eng. Archit. GAZI **31**(3), 567–578. doi:https://doi.org/10.17341/gummfd.81389
9. De Cooman B, Chin K, Kim J (2011) High Mn TWIP steels for automotive applications. New Trends and Developments in Automotive System Engineering, InTech, 101–128
10. Chung K, Ahn K, Yoo D-H, Chung K-H, Seo M-H, Park S-H (2011) Formability of TWIP (twinning induced plasticity) automotive sheets. Int J Plasticity 27(1):52–81. https://doi.org/10.1016/j.ijplas.2010.03.006

11. Habibi N, Zarei-Hanzaki A, Abedi H-R (2015) An investigation into the fracture mechanisms of twinning-induced-plasticity steel sheets under various strain paths. J. Mater. Process Tech. 224(1): 102–116. https://doi.org/10.1016/j.jmatprotec.2015.04.014
12. Han HN, Kim K-H (2003) A ductile fracture criterion in sheet metal forming process. J. Mater. Process Tech. 142(1):231–238. https://doi.org/10.1016/S0924-0136(03)00587-9
13. Lou Y, Huh H (2013) Prediction of ductile fracture for advanced high strength steel with a new criterion: experiments and simulation. J Mater Process Tech 213(8):1284–1302. https://doi.org/10.1016/j.jmatprotec.2013.03.001
14. Xu L, Barlat F, Lee M-G (2012) Hole expansion of twinning-induced plasticity steel. Scripta Mater 66(12):1012–1017. https://doi.org/10.1016/j.scriptamat.2012.01.062
15. Xu L, Chen L, De Cooman BC, Steglich D, Barlat F (2010) Hole expansion of advanced high strenth steel sheet sample. Int J Mater Form 3(1):247–250. https://doi.org/10.1007/s12289-010-0753-9
16. Ahn K, Yoo D, Seo MH, Park S-H, Chung K (2009) Springback prediction of TWIP automotive sheets. Met Mater Int 15(4):637–647. https://doi.org/10.1007/s12540-009-0637-z
17. Hill R (1948) A theory of the yielding and plastic flow of anisotropic metals. Proceedings of the Royal Society of London Series A Mathematical and Physical Sciences 193(1033):281–297
18. Barlat F, Lian K (1989) Plastic behavior and stretchability of sheet metals. Part I: A yield function for orthotropic sheets under plane stress conditions Int J Plasticity 5(1):51–66. https://doi.org/10.1016/0749-6419(89)90019-3
19. Barlat F, Brem JC, Yoon JW, Chung K, Dick RE, Lege DJ, Pourboghrat F, Choi SH, Chu E (2003) Plane stress yield function for aluminum alloy sheets—part 1: theory. Int. J. Plasticity 19(9): 1297–1319. https://doi.org/10.1016/S0749-6419(02)00019-0
20. Banabic D, Balan T, Comsa DS (2000) A new yield criterion for orthotropic sheet metals under plane-stress conditions. In: proceedings of the 7th conference 'TPR2000', Cluj Napoca, Romania, pp. 217–224
21. Hashimoto K, Kuwabara T, Iizuka E, Yoon JW (2010) Hole expansion simulation of high strength steel sheet. Int J Mater Form 3(1):259–262. https://doi.org/10.1007/s12289-010-0756-6
22. Barlat F, Aretz H, Yoon JW, Karabin ME, Brem JC, Dick RE (2005) Linear transfomation-based anisotropic yield functions. Int. J. Plasticity 21(5):1009–1039. https://doi.org/10.1016/j.ijplas.2004.06.004
23. Toros S, Polat A, Ozturk F (2012) Formability and springback characterization of TRIP800 advanced high strength steel. Mater. Design. 41:298–305. https://doi.org/10.1016/j.matdes.2012.05.006
24. Ozturk F, Toros S, Kilic S, Kacar I (2014) Evaluation of anisotropy by two different tests for TRIP800 steel. In: key engineering materials, pp. 1139-1144. Trans Tech Publ
25. Ozturk F, Lee D (2005) Experimental and numerical analysis of out-of-plane formability test. J. Mater. Process Tech. 170(1–2): 247–253. https://doi.org/10.1016/j.jmatprotec.2005.05.010
26. Asame Co.: Automated Strain Analysis and Measurement Environment. http://www.techlab.fr/ (Accessed 2 Apr 2015). 01.01.2016
27. Ozturk F, Dilmec M, Turkoz M, Ece RE, Halkaci HS (2009) Grid marking and measurement methods for sheet metal formability. In: the 5th international conference and exhibition on design and production of machines and dies/molds, Turkey, June, pp. 18–21
28. Tresca H (1864) Memoire sur l'écoulement des solides à de forte pressions. Acad Sci Paris 2(1):59
29. Mises RV (1913) Mechanik der festen Körper im plastisch-deformablen Zustand. Nachrichten von der Gesellschaft der Wissenschaften zu Göttingen, Mathematisch-Physikalische Klasse 1913(1):582–592
30. Banabic D (2010) Sheet metal forming processes: constitutive modelling and numerical simulation. Springer Berlin Heidelberg, Berlin
31. Fallahiarezoodar A, Altan T (2015) Determining flow stress data by combining uniaxial tensile and biaxial bulge tests. Stamping Journal **1**(1)
32. Marciniak Z (1965) Stability of plastic shells under tension with kinematic boundary condition. Archiwum Mechaniki Stosorwanej 17(0):577–592
33. Marciniak Z, Kuczyński K (1967) Limit strains in the processes of stretch-forming sheet metal. Int J Mech Sci 9(9):609–620. https://doi.org/10.1016/0020-7403(67)90066-5
34. Azrin M, Backofen WA (1970) The deformation and failure of a biaxially stretched sheet. MT 1(10):2857–2865. https://doi.org/10.1007/BF03037824
35. Banabic D (2010) A review on recent developments of Marciniak-Kuczynski model. Computer Methods in Materials Science 10(4): 225–237
36. Hutchinson JW, Neale KW (1978) Sheet necking-III. Strain-rate effects. In: Koistinen DP, Wang N-M (eds) Mechanics of sheet metal forming: material behavior and deformation analysis. Springer US, Boston, MA, pp 269–285
37. Ghazanfari, A., Assempour, A.: Calibration of forming limit diagrams using a modified Marciniak–Kuczynski model and an empirical law. Mater Design 34(0), 185–191 (2012). doi:https://doi.org/10.1016/j.matdes.2011.07.057
38. Ozturk F, Toros S, Kilic S (2014) Effects of anisotropic yield functions on prediction of forming limit diagrams of DP600 advanced high strength steel. Procedia Engineering 81(1):760–765. https://doi.org/10.1016/j.proeng.2014.10.073